energies

MDPI

Review

A Comprehensive Review on Two-Step Thermochemical Water Splitting for Hydrogen Production in a Redox Cycle

Daphne Oudejans [1], Michele Offidani [1,2,3], Achilleas Constantinou [4], Stefania Albonetti [2,3], Nikolaos Dimitratos [2,3] and Atul Bansode [1,*]

[1] Catalysis Engineering, Department of Chemical Engineering, Delft University of Technology, Van der Maasweg 9, 2629 HZ Delft, The Netherlands; d.g.oudejans@student.tudelft.nl (D.O.); micheleoffidani@gmail.com (M.O.)
[2] Department of Industrial Chemistry "Toso Montanari", University of Bologna, Viale Risorgimento 4, 40136 Bologna, Italy; stefania.albonetti@unibo.it (S.A.); nikolaos.dimitratos@unibo.it (N.D.)
[3] Center for Chemical Catalysis—C3, Alma Mater Studiorum Università di Bologna, Viale Risorgimento 4, 40136 Bologna, Italy
[4] Department of Chemical Engineering, Cyprus University of Technology, Limassol 3036, Cyprus; axilleas.constantinou@ucl.ac.uk
* Correspondence: a.b.bansode@tudelft.nl; Tel.: +31-1527-81060

Abstract: The interest in and need for carbon-free fuels that do not rely on fossil fuels are constantly growing from both environmental and energetic perspectives. Green hydrogen production is at the core of the transition away from conventional fuels. Along with popularly investigated pathways for hydrogen production, thermochemical water splitting using redox materials is an interesting option for utilizing thermal energy, as this approach makes use of temperature looping over the material to produce hydrogen from water. Herein, two-step thermochemical water splitting processes are discussed and the key aspects are analyzed using the most relevant information present in the literature. Redox materials and their compositions, which have been proven to be efficient for this reaction, are reported. Attention is focused on non-volatile redox oxides, as the quenching step required for volatile redox materials is unnecessary. Reactors that could be used to conduct the reduction and oxidation reaction are discussed. The most promising materials are compared to each other using a multi-criteria analysis, providing a direction for future research. As evident, ferrite supported on yttrium-stabilized zirconia, ceria doped with zirconia or samarium and ferrite doped with nickel as the core and an yttrium (III) oxide shell are promising choices. Isothermal cycling and lowering of the reduction temperature are outlined as future directions towards increasing hydrogen yields and improving the cyclability.

Keywords: hydrogen; two-step thermochemical water splitting; redox cycles; temperature swing; pressure swing; isothermal cycling; cyclability

Citation: Oudejans, D.; Offidani, M.; Constantinou, A.; Albonetti, S.; Dimitratos, N.; Bansode, A. A Comprehensive Review on Two-Step Thermochemical Water Splitting for Hydrogen Production in a Redox Cycle. *Energies* **2022**, *15*, 3044. https://doi.org/10.3390/en15093044

Academic Editors: Antonino S. Aricò and Muhammad Aziz

Received: 26 February 2022
Accepted: 18 April 2022
Published: 21 April 2022

1. Introduction

Over the past few years, there has been great interest in sustainable carbon-free fuels. A large portion of the fuels used nowadays are fossil fuels, which have high energy density levels and with which carbon dioxide is emitted upon utilization. The consequences of such emissions are now becoming increasingly visible by means of increased carbon dioxide concentrations in the atmosphere, which are highly comparable to those 3–4 million years ago. During those times, the earth's average temperature was ca. 3 °C higher and the sea levels were ca. 25 m higher than now. The dire consequences of such drastic environmental changes are well documented [1]. Therefore, a more sustainable energy alternative is needed in order to reduce carbon dioxide emissions and limit the impacts of fuels on the environment. Owing to the finite nature of fossil fuels, there has been growing interest in renewable carbon-free fuels, such as hydrogen. Hydrogen can be produced using

water [2,3] and energy-dense [4,5]. Hydrogen can either be used in fuel cells or in internal combustion engines [6–8]. In fuel cells, hydrogen is split into H^+ and electrons at the anode. These electrons flow through an external circuit to generate a current and then flow to the cathode, where they form water with H^+ and oxygen [9,10]. In internal combustion engines, hydrogen is combusted with oxygen, which generates water and heat [6–8]. In both cases, only water is formed and no carbon dioxide or any other environmental pollutants are generated.

Although hydrogen is often proposed as a sustainable alternative, this largely depends on the method with which the hydrogen is produced [11]. How sustainable hydrogen is, depending on the energy source, is indicated by three main colors: grey, blue or green [12]. The most polluting variant is grey hydrogen, because fossil fuels are utilized in the production of hydrogen. Blue hydrogen is also produced using fossil fuels, but the difference compared to grey hydrogen is that the produced carbon dioxide is captured and stored, such that the impact on the environment is reduced. The most sustainable type of hydrogen is green hydrogen. In order to receive this grading, the hydrogen should be produced from 100% renewable energy [12,13]. There are several different pathways through which hydrogen can be generated. Steam reformation of fossil fuels is currently the major pathway for hydrogen production. In the process of steam reforming, the fossil fuels react with water to produce hydrogen, carbon monoxide and some carbon dioxide. In order to enrich the hydrogen phase, the water–gas shift reaction is often performed after reformation. In this reaction, carbon monoxide and water are in equilibrium with hydrogen and carbon dioxide [14]. Although producing hydrogen in this way is relatively cheap [4,14,15], greenhouse gases are emitted and fossil fuels are utilized, such that this hydrogen is classified as grey hydrogen, meaning this method can no longer be regarded as sustainable. Biomass gasification is another method proposed for hydrogen production. In this process, the biomass reacts with steam or air to generate hydrogen. Theoretically, this synthesis method has a very large feedstock [16], but many impurities can be present in the feedstock [15], which induces operational difficulties. Next to hydrogen and carbon monoxide, methane and carbon dioxide are formed [17], both of which are greenhouse gases that contribute to global warming. Although renewable hydrogen is produced, the fuel is not carbon-free, since carbon-containing gases are indirectly emitted.

Alternatively, hydrogen can also be produced through currently popular approaches, such as electrolysis and photo-assisted water splitting methods, provided that green electricity is used [16]. The past decades have seen extensive efforts regarding hydrogen production via water splitting reaction by employing different strategies, such as photo-, electro-, photo-electro- or thermo-based methods. Electrolysis, photolysis and combined photoelectrochemical water splitting for the production of hydrogen are a few of the actively investigated research topics in the field of renewable energy research. For electrolysis-based systems, polymer electrolyte membrane electrolyzers have attracted much attention due to their compactness, quick response times and improved current densities [18]. The photolysis method has been considered as a thorough solution as it utilizes solar energy, either directly or in the form of electricity, to produce hydrogen [19]. Despite the progress in renewable hydrogen production methods, the majority (95%) of hydrogen is still coming from non-renewable sources, and water splitting only accounts for 3.9% of the total hydrogen production [20]. In order to fulfil the future needs for green hydrogen production, it is imperative to explore all possible pathways to harness hydrogen from water by using renewable energy sources [15,21,22].

Among others, thermochemical water splitting [23] is an attractive way of using thermal energy, either from solar radiation by concentrating the sunlight or from renewable electricity in remote locations for hydrogen generation [4,24–26]. The features of the hydrogen production methods discussed here are summarized in Table 1. The thermal decomposition of water into hydrogen and oxygen occurs at temperatures higher than 2000 °C [27], although the utilization of redox materials to create the reduction and oxidation cycles can effectively lower the temperature requirements down to 1000 °C [28–30].

Such redox-material-based thermochemical water splitting reaction cycles can be caried out within a temperature range of 900–1500 °C, with successive higher and lower temperature steps in cycles. The thermochemical water splitting cycle contains two reactions given by Equations (1) and (2) [31] with M, Ce, Fe, Mg, Sn or Zn [4,25,32–34]. The first reaction is the thermal reduction of the redox material at a temperature typically higher than the oxidation reaction (Equation (2)) [2,31,35,36] to generate oxygen and oxygen vacancies within the redox material. Subsequently, the reduced redox material reacts with water to regenerate the redox material, as well as to generate hydrogen. Since oxygen and hydrogen are produced in two different reactions, the separation of both gases is not required [31,37], and the hydrogen produced via this approach can be directly utilized as a fuel [35]. The reduction reaction is endothermic and is favored at elevated temperatures. Since the oxidation reaction is exothermic, it is preferably operated at a temperature lower than the reduction reaction to increase the hydrogen yield [31]:

$$MO_x \rightarrow MO_{x-\delta} + \frac{\delta}{2}O_2 \quad (1)$$

$$MO_{x-\delta} + \delta H_2O \rightarrow MO_x + \delta H_2 \quad (2)$$

Table 1. Overview of hydrogen production methods, including the feed, energy source and major advantages and challenges.

Hydrogen Production Method	Feed	Energy Source	Major Advantages	Major Challenges
Steam reforming	Fossil fuels	Thermal	- Cheap Production - Already commercially implemented	- Greenhouse gases are emitted - Fossil fuels are depleted
Biomass gasification	Biomass	Thermal	- Large feedstock - Conventional equipment can be used	- Impurities in the feed induce difficulties - Greenhouse gases are emitted
Electrolysis	Water	Electricity	- Abundant feed - No emissions - Integration with renewable energy	- Large electricity consumption - Difficulties in storage and transport
Photolysis	Water	Photonic	- Abundant feed - No emissions - Conversion of solar energy to hydrogen	- Low efficiency - Difficult to scale-up - Requires for sunlight (differs in different areas of the world)
Photoelectrochemical	Water	Electricity + photonic	- Abundant feed - No emissions - Less power required compared to photolysis	- Low efficiency - Difficult to scale-up - Requires for sunlight (differs in different areas of the world)
Thermochemical	Water	Thermal	- Abundant feed - Large-scale hydrogen production - Utilization of waste heat	- Requires heat-resistant materials - Slow heating–cooling cycles - Thermal losses

Herein, we describe the current state of the art in the thermochemical water splitting route for hydrogen production through two redox cycles, covering several important aspects. Excellent reviews have been published summarizing the aspects of such reactions, although individually. The thermodynamics of the reaction along with a comparison between the most promising materials were discussed by Mao et al. [38]. A variety of possible solar reactors and a thermodynamic analysis of solar thermochemical processes, including solar efficiency, was reported by Steinfeld et al. [39]. An in-depth discussion on perovskites, a promising class of materials, was carried out by Abanades et al. [40]. They also focused their attention on thermodynamic and kinetic aspects of thermochemical cycles. Other information on the most promising materials applicable to thermochemical water splitting cycles can be found in the literature [25,41]. Nevertheless, as far as we know, there is still a lack of a work covering all of the different aspects and summarizing them through a rational comparison of the main information present in the literature. The aim of the present review is to present the current knowledge related to thermochemical water splitting in order to provide a general overview of the topic and to present future prospects in a single review. At first, the thermodynamics of water splitting cycles using metal oxides is presented, then the most promising reactors applicable to thermochemical water splitting are discussed, which are divided according to the method used to reach the operating temperature. Each system is described and critically analyzed, highlighting its advantages and drawbacks. Next, the most promising redox materials are examined, focusing attention on the main methods with which it is possible to improve their performance (e.g., doping with other metals, the use of supports or morphology controls). A multi-criteria analysis is also included in this work in order to compare the different materials previously reported in the literature. Moreover, the current work provides a direction for future research based on the rational understanding of the different aspects involved in thermochemical water splitting for hydrogen generation using mainly non-volatile redox materials.

2. Hydrogen Production through Thermochemical Water Splitting

2.1. Thermodynamics of Water Splitting Cycles Using Metal Oxides

Studying the thermodynamics of a thermochemical water splitting cycle allows one not only to determine how the different variables affect the reactions but also how to act on them to drive the reaction forward. In the literature, two-step thermochemical water splitting cycles were treated both as closed and open systems [31,38,40]. The first approach is the easier one and also the most reported. In a closed system, no mass transfer can occur with the surrounding environment and only energy transfer is possible. In such cases, the Gibbs standard free energy for the reduction and the subsequent oxidation step can be expressed with Equations (3) and (4):

$$\Delta G_{TR,T_{TR}} = \Delta H_{red} - T_{TR} \cdot \left(\Delta S_{red} + \frac{1}{2} S^{O_2}_{T_{TR}} \right) \leq 0 \quad (3)$$

$$\Delta G_{WS,T_{WS}} = -\Delta H_{red} - \Delta H^{H_2O}_{f,T_{WS}} - T_{WS} \cdot \left(S^{H_2}_{T_{WS}} - S^{H_2O}_{T_{WS}} - \Delta S_{red} \right) \leq 0 \quad (4)$$

where ΔG is the Gibbs free energy variation, and ΔH_{red} and ΔS_{red} are, respectively, the enthalpy and entropy changes of the metal oxide caused by the reduction. T is the temperature expressed in kelvins and S^i is the formation entropy for the specified compound. TR stands for the thermal reduction step, whereas WS stands for water splitting. The temperatures of the two steps are indicated by T_{TR} and T_{WS}, where the first refers to the thermal reduction and the latter to the water splitting step [31,38].

Rearranging the previous two equations, it is possible to calculate the ΔT values between the reduction and oxidation steps, as in Equation (5):

$$\Delta T = \frac{-2\Delta G^{H_2O}_{f,T_{WS}} - T_{WS} \cdot \Delta S}{S^{O_2}_{T_{TR}} + 2\Delta S_{red}} \quad (5)$$

where $\Delta G_{f,T_{WS}}^{H_2O}$ is the Gibbs free energy change for the water formation reaction and ΔS is the entropy increase in O_2 when it is heated from T_{WS} to T_{TR}.

Thus, by modeling the reactor as a closed system, the process is only possible if a minimum temperature difference between the two steps is provided. By analyzing Equations (3) and (5), it is also possible to observe that an ideal redox material should have a low enthalpy variation (ΔH_{red}) to favor the reduction step, even at lower temperatures, and a high entropy variation (ΔS_{red}) to ensure a small ΔT [31].

Modeling the process as an open system allows one to take into account the flows that are going into and out of the reactor. An open system, indeed, is defined as a system in which both energy exchange and mass transfer with the environment is possible. The general definition of the Gibbs free energy, as reported in Equation (6), can be applied in this case [31]:

$$G = PV - TS + \sum_{j=1}^{M} \mu_j \cdot N_j \quad (6)$$

where G is the Gibbs free energy; P, V, T and S are the pressure, volume, temperature and entropy, respectively; μ_j is the chemical potential of species j; N_j is the number of species j, while the sum is taken over all relevant species.

In order for the hydrogen evolution step to occur, the Gibbs free energy of the reactants must be higher than that of the products, as expressed in Equation (7). The total pressure and volume of the system are considered constants:

$$-T_{TR}\left(S_{H_2O} + S_{MO_{x-\delta}}\right) + \mu_{H_20}N_{H_20} + \mu_{MO_{x-\delta}}N_{MO_{x-\delta}} > -T_{TR}\left(S_{H_2} + S_{MO_x}\right) + \mu_{H_2}N_{H_2} + \mu_{MO_x}N_{MO_x} \quad (7)$$

Since the reaction takes place on a solid redox material, the numbers of molecules in the previous equations are referenced to the number adsorbed on the surface of the solid. By isolating the water chemical potential and expressing the number of adsorbed molecules as a function of the partial pressure Equation (8), it is possible to obtain Equation (9):

$$N_j = \alpha_j \cdot P_j \quad (8)$$

$$\mu_{H_20}\alpha_{H_20}P_{H_20} > -T_{TR}\left(S_{H_2} + S_{MO_x} - S_{H_2O} - S_{MO_{x-\delta}}\right) + \mu_{H_2}\alpha_{H_2}P_{H_2} + \mu_{MO_x}N_{MO_x} - \mu_{MO_{x-\delta}}N_{MO_{x-\delta}} \quad (9)$$

where α_j and P_j are, respectively, Henry's adsorption coefficient and the partial pressure of species j. From Equation (9), it is clear how an increase in P_{H_20} along with a contextual decrease in P_{H_2} can drive forward the reaction, without any changes in temperature. Thus, an isothermal approach is possible by operating at a temperature above the minimum one needed for the reduction of the redox material. During the oxidation step, the incoming flow swipes away the hydrogen generated, providing the driving force for the hydrogen evolution reaction [31].

2.2. Reactor Systems and Methodologies

The reactor system where the redox cycles can be carried out is at the core of this water splitting route. Due to the high temperature requirements and cycling between different temperatures (for two-step thermochemical water splitting), selecting an appropriate reactor is essential. Over the years, various reactor designs have been demonstrated and used for research relating to two-step thermochemical water splitting for hydrogen generation using redox cycling. Some promising and interesting reactor designs are presented and discussed below. A distinction is made based on the method used to reach the desired temperature. Firstly, multiple reactor designs utilizing solar light for thermochemical water splitting are discussed, followed by infrared reactors. These are the two types of reactors frequently used for studying thermochemical water splitting. Lastly, the use of a microwave oven as a reactor for this system is discussed.

2.2.1. Solar Reactors

Solar reactors have conventionally been used for such reactions, as temperatures up to 2000 °C can be reached, which are beneficial for the reduction of the redox material. In order to collect the solar energy, the solar light must first be concentrated. The concentrated light is then reflected onto a receiver where the temperature is reached [38,42]. Concentration of the solar light is achieved through a heliostat field or a parabolic dish system. These two technologies are well-developed and their schematics are shown in Figure 1 [38]. Although these high temperatures are required to reach high hydrogen production rates, a major drawback is that the solar radiation can damage the samples, for example through degradation [43].

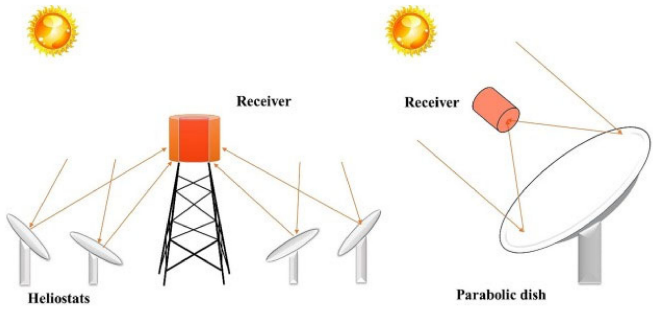

Figure 1. Schematic representation of a heliostat field (**left**) and a parabolic dish system (**right**), which are two well-developed technologies used to concentrate sunlight [38].

Figure 2 describes the solar setup proposed by Chueh et al. to carry out the thermochemical water splitting cycles over ceria [44]. The concentrated sunlight passes through a quartz window and is concentrated onto the sample. The reduction reaction was performed at a temperature of approximately 1600 °C for 1 h in argon, whereas at 500 °C the hydrogen was generated by passing a gaseous mixture of argon and water for about 30 min over the reduced redox material. In the same research, the performance of the solar reactor for thermochemical cycling of ceria for hydrogen generation was compared to the performance using an infrared furnace. The conditions slightly differed as higher flow rates could be attained in the furnace. Furthermore, the reduction reaction was performed at 1500 °C for 20 min and the oxidation reaction was performed at 800 °C for 10 min. It was found that higher generation rates for oxygen and hydrogen could be reached using an infrared furnace compared to the solar reactor. An additional advantage of the furnace over the solar reactor was that a stable temperature could be maintained [44]. Reactors using an infrared furnace are discussed in more detail in the next section.

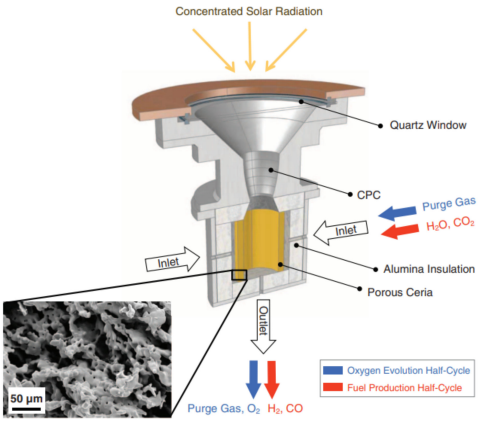

Figure 2. Schematic representation of the solar reactor used for thermochemical water splitting. The redox material used in porous ceria. As the same setup was used in another experiment for syngas production, carbon dioxide and carbon monoxide are also denoted in the figure, as well as a scanning electron microscope image of ceria after 23 cycles. Reprinted from [44].

In a setup similar to the one shown in Figure 2, Fe_3O_4 was reduced to FeO in a report by Charvin et al. The sample was placed in the solar reactor and cooled by water. During the reduction reaction, nitrogen was supplied to the reactor. Only the reduction reaction was performed in the solar reactor, while the oxidation reaction was carried out in an electrical furnace to reach temperatures below 800 °C, which are preferred for this reaction type according to its thermodynamics. Steam carried by argon was supplied to the furnace containing the sample. A schematic representation of the setup used for water splitting is shown in Figure 3 [45].

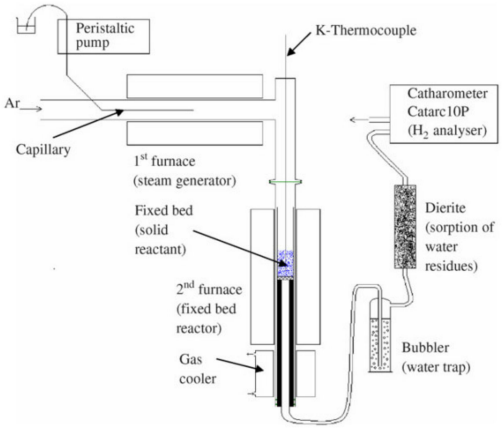

Figure 3. Schematic representation of the experimental setup used for the oxidation of FeO to Fe_3O_4 for hydrogen production. Reprinted from [45].

Oliveira et al. reported on a solar reactor used for thermochemical cycling of cork-templated ceria. The samples were placed in an alumina tube and then placed in the solar reactor. In contrast to the setup shown in Figure 2, the concentrated solar light entered the reactor from the side instead of from the top. The reduction temperature was 1400 °C and the reaction took place while argon was passed over the sample. At the end of the reduction process, the material was marked by low and constant oxygen generation for 15 min. The temperature was then lowered by not supplying any solar radiation to the reactor and without additional cooling. When the oxygen concentration was approximately zero, a gaseous mixture of argon and water was supplied to the reactor and the oxidation reaction took place. A schematic representation of the reactor is shown in Figure 4 [42].

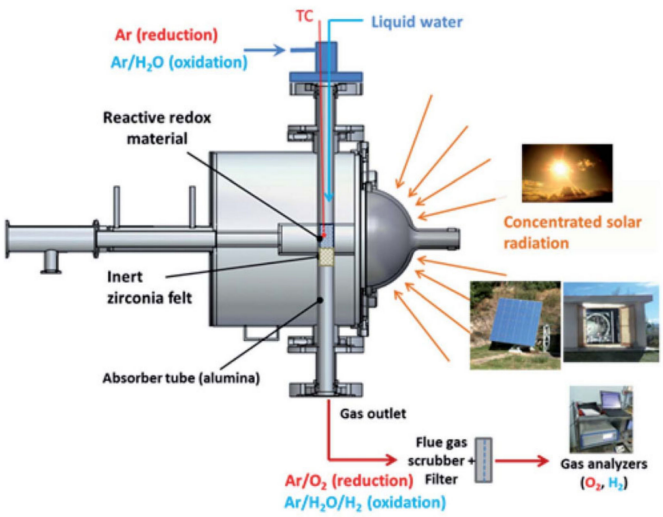

Figure 4. Schematic representation of a solar reactor used for thermochemical redox cycling of cork-templated ceria. The reduction temperature was 1400 °C and the oxidation reaction took place during free cooling when the oxygen concentration dropped to approximately zero. Reprinted from [42].

A solar reactor was reviewed by Al-Shankiti et al. for isothermal and thermochemical water splitting [46]. The reactor is a packed bed reactor, where the bedding is indirectly radiated by solar light. Either steam or an inert gas can be supplied to the bed through different openings. The main disadvantage of this reactor is the non-uniformity of the temperature profile inside the reactor, which can be mitigated by fluidizing the particles. The reactor's schematic representation is shown in Figure 5 where numbers from 1 to 6 are the fixed bed reactor tubes.

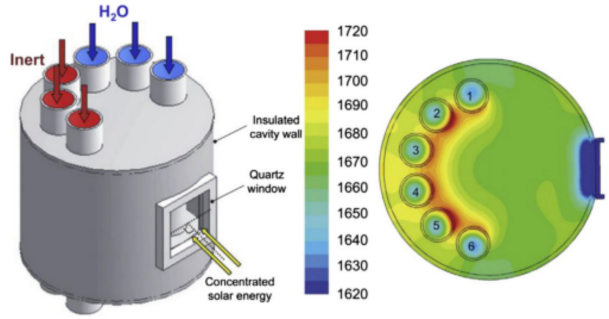

Figure 5. Isothermal reactor used for thermochemical water splitting. Reprinted from [47].

Figure 6 shows a schematical representation of a solar reactor with fluidized particles, as used by Kodama et al. The solar radiation passing through the quartz window directly heats the particles, such that the bed can reach temperatures of up to 1400 °C. Due to the fluidization of the bed, the heated particles move down, while the unheated particles move up towards the quartz window. As the particles move counter-currently, heat can be exchanged. In order to conduct reduction and oxidation reactions for hydrogen production using two-step thermochemical water splitting, the gas flow is either nitrogen or steam for the reduction and oxidation reaction, respectively. The temperature of the bed is changed from 1400 °C to 1000 °C upon steam injection [48]. This reactor design was used as inspiration for an experimental setup proposed by Gokon et al. for the thermal reduction of $NiFe_2O_4$ supported on monoclinic zirconia. The subsequent water splitting step was carried out in the setup shown in Figure 7b [49].

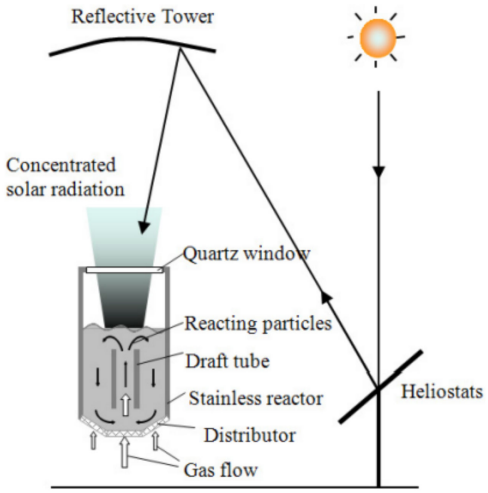

Figure 6. Fluidized-bed solar reactor for two-step thermochemical water splitting. The reduction reaction takes place in a nitrogen atmosphere at 1400 °C and steam is supplied for the oxidation reaction, which is conducted at 1000 °C. Reprinted from [48].

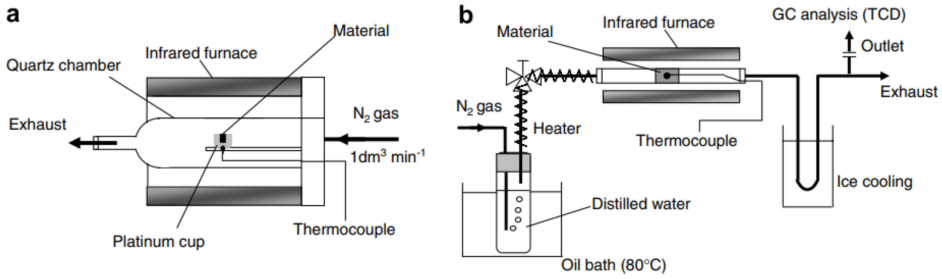

Figure 7. Schematic representation of the experimental setup used for (**a**) thermochemical reduction of Fe_3O_4 supported on yttria-stabilized zirconia and $Ni_xFe_{3-x}O_4$ supported on monoclinic zirconia, as well as (**b**) oxidation of $Ni_xFe_{3-x}O_4$ supported on monoclinic zirconia. The reduction temperature was 1400 °C and the oxidation temperature was 1000 °C for both redox materials. Reprinted from [50].

2.2.2. Infrared Reactors

Experiments have been conducted using an infrared furnace as a reactor, because the main advantage of this reactor type over the solar reactors is that the temperature can more easily be controlled. Although the maximum temperature that can be reached using these furnaces is lower compared to solar reactors, it has been found that reasonable hydrogen production (around 15 mL/g·cycle, [50]) is attained, as follows from the examples discussed below. Furthermore, these high temperatures are no longer required due to current research being focused on lowering the reduction temperature, among others. Kodama et al. reported a setup where the sample is placed in a platinum cup, which is then placed on a ceramic bar in a quartz tube. The redox material, Fe_3O_4 supported on yttrium-stabilized zirconia, was reduced at 1400 °C for 1 h while a nitrogen flow was passed over the redox material. After the reduction reaction, the sample was cooled down to room temperature. Before conducting the oxidation step, the sample was pulverized. The oxidation reaction was performed at 1000 °C for 50 min. The temperature was changed from room temperature to 1000 °C within 10 min. A gaseous mixture of nitrogen and water flowed through the reactor. In this experimental setup, the temperature of the reduction reaction was controlled using an R-type thermocouple. A K-type thermocouple was used to control the temperature of the oxidation reaction. A schematic representation of the setup used for thermochemical reduction is shown in Figure 7a [30]. The setup as shown in Figure 7 was used for another study by Kodama et al., where nickel-doped Fe_3O_4 supported on monoclinic-zirconia was analyzed for thermochemical water splitting. The setups for the reduction and oxidation reactions are shown in Figure 7a,b, respectively. The reduction reaction took place at 1400 °C over 10 min in a nitrogen atmosphere. The sample was cooled down after the reduction reaction and pulverized, in agreement with the above discussed above for thermochemical redox cycling of Fe_3O_4 supported on yttrium-stabilized zirconia. The oxidation temperature, which was 1000 °C, was reached within 10 min. The oxidation reaction was performed for 60 min while a gaseous mixture of nitrogen and water was passed over the sample. The same thermocouples were used for controlling the temperatures of the different reactions as for yttrium-stabilized, zirconia-supported Fe_3O_4 [50].

Instead of an infrared furnace, a vertical split electrical furnace was used by Bhosale et al. A schematic representation of the setup is shown in Figure 8. The reduction reaction of nickel-doped ferrites took place at 900 °C in a nitrogen atmosphere. After 2 h, steam carried by nitrogen was supplied to the reactor. The oxidation temperature was altered, and it was found that oxidation at 900 °C results in the highest average hydrogen production per cycle (40 mL/g·cycle). However, the hydrogen production dropped quickly over four cycles due to sintering [51].

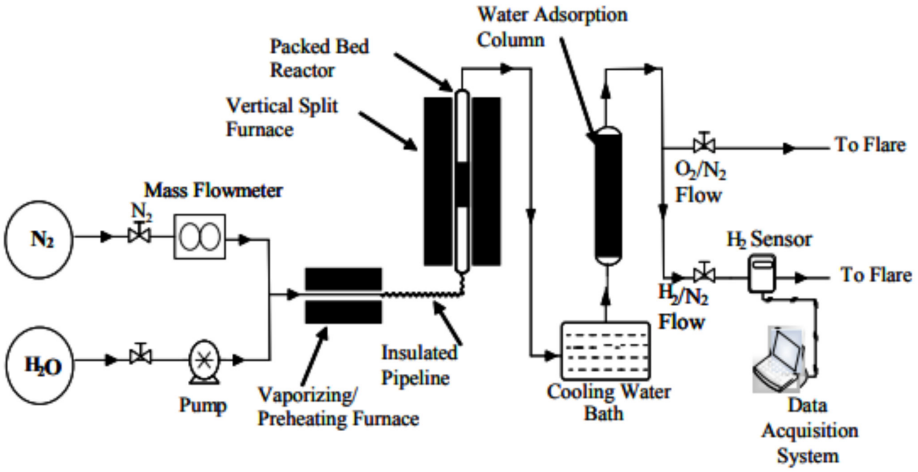

Figure 8. Schematic representation of the experimental setup used for thermochemical water splitting for hydrogen generation. Reprinted from [51].

The same experimental setup as shown in Figure 8 was also used for hydrogen production from zirconium-doped ferrites in another study by Bhosale et al. The reduction reaction was found to only be possible for temperatures above 1050 °C, while the water splitting reaction could be performed at 800 °C [52]. Tin-doped ferrites were also investigated by Bhosale et al., for which the same setup was again used. At 1100 °C the reduction reaction was performed, while the oxidation reaction was performed at 900 °C [53]. The setup shown in Figure 8 was also reported by Bhosale et al. for manganese-doped ferrites. The influence of the reduction and oxidation temperatures on the hydrogen yield was investigated. It was concluded that reduction at 1100 °C and oxidation at 900 °C results in the highest hydrogen yield over multiple cycles (8.44 mL/g·cycle) [54].

2.2.3. Microwave Oven

The thermochemical water splitting reaction can also take place in a microwave oven, which can be used to heat the sample [55]. The advantage of the use of microwave ovens over other heating methods is that they are known for their fast and effective heating [56]. However, a major disadvantage is that microwave ovens are uncontrollable, which leads to unreliable temperature measurements as well as temperature gradients in the sample [56,57]. It was shown that a microwave oven could successfully be used for hydrogen production via the thermochemical water splitting cycle. In the specific setup reported by Gao et al., the sample is placed in a quartz reactor, which is then placed inside the microwave oven. The reduction step takes place in an inert nitrogen environment upon microwave irradiation. For the oxidation reaction, a mixture of nitrogen and water is passed over the sample in the microwave oven. The sample used in the study was $(FeMgCoNi)O_x$ supported on a silicon carbide foam [55]. This material is a poly-cation oxide. Although poly-cation oxides are not discussed in detail in this paper, the experimental setup has still been included as it could theoretically also be used for the redox materials discussed in this paper. The experimental setup used for this particular research also includes several other devices, such as an oscilloscope to measure the microwave light intensity. The water trap and silica gel in between the microwave oven and the gas chromatograph prevent the passing of unreacted water to the gas chromatograph, since this can possibly damage the device. Figure 9 shows a schematic representation of the setup used in this research [55].

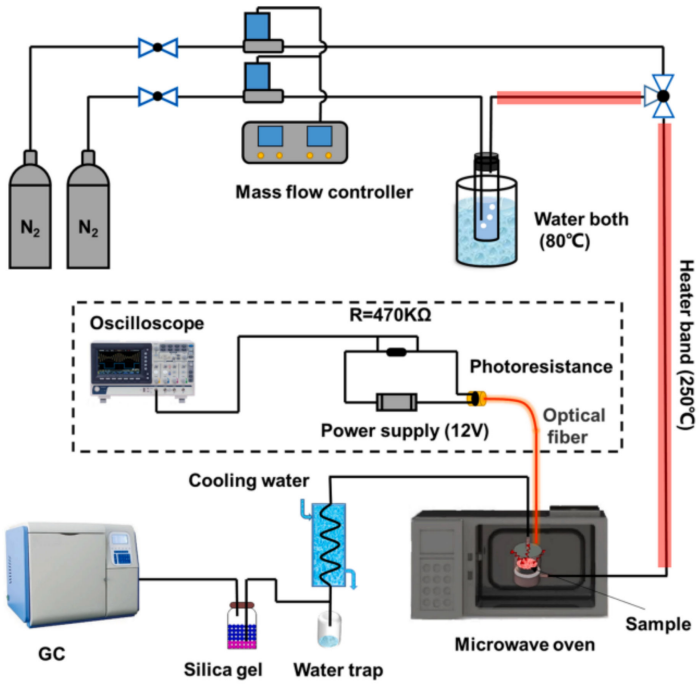

Figure 9. Schematic representation for performing the thermochemical water splitting cycle using $(FeMgCoNi)O_x$ supported on silicon carbide foam using a microwave oven. Reprinted from [55].

In the research discussed above, the reduction reaction took 4 min, and the gaseous mixture of nitrogen and water was passed over the sample for 30 min in order to oxidize the sample. The fastest oxygen generation rate was found at a power of 900 W, which corresponded to a temperature of approximately 650 °C. Although the fastest oxygen generation rate was reached at a power of 900 W, the fastest hydrogen generation rate was obtained for a power of 700 W. At this power, the highest oxygen and hydrogen yields were also obtained. At 700 W, a temperature of 600 °C could be reached [55].

2.3. Temperature Swing vs. Pressure Swing Cycling

The two-step thermochemical water splitting redox cycle has conventionally been treated as a closed system. Analyzing this system using thermodynamics by assuming a closed system shows that there is a minimal temperature difference required in order to drive the reduction and oxidation reaction. However, there are some challenges related temperature swing, such as thermal losses, slow heating and cooling rates and thermal stress on the materials upon cycling [31,46,58]. It is highly desirable to use a different mode of operation that does not have these disadvantages or alleviates them.

Recent studies have shown that it is possible to operate the cycle isothermally by using a pressure swing instead of a temperature swing [31,59]. This new approach solves some of the challenges of the temperature swing approach, such as limiting thermal losses and the thermal stress on the materials. It was shown by assuming an open system that isothermal operation is possible because oxygen, unreacted water and hydrogen are removed from the system. During isothermal operation, the reactions are driven by ensuring the high partial pressure of water during the oxidation reaction and the low partial pressure of oxygen while the redox material is reduced, such that the Gibbs free energy of the reactants exceeds the Gibbs free energy of the products [31,46]. Oxygen and hydrogen should, thus, continuously be removed from the system along with unreacted water in order to drive the reactions to the right and obtain a reasonable hydrogen yield. However, keeping the partial pressure of water high and the partial pressure of oxygen low could be a challenge. The theoretical efficiency of the pressure swing operation is also lower compared to traditional temperature swing operations, as the reactions are not operated at their most favorable

temperatures [60,61]. Another challenge induced by isothermal redox cycling is that excess steam needs to be added in order to regenerate the redox material [46,62,63]. Although the amount of excess steam required for oxidation depends on the isothermal operating temperature, it has been reported that the ratio of hydrogen produced to steam required is much smaller than 1 ($n_{hydrogen}$:n_{steam} << 1). For the temperature swing operation, this ratio is around or close to 1 [62].

According to computational studies, the isothermal operation should attain a temperature higher than 1300 °C in order to outperform the temperature swing approach in terms of efficiency [64]. It has been reported that isothermal cycling results in faster kinetics compared to the temperature swing approach, where the isothermal operating temperature is equal to the reduction temperature for the other operation mode [46]. From the simulations, it was concluded that heat recovery solely from the outgoing gases for the temperature swing approach is insufficient to outperform the efficiency of an isothermal cycle, although if heat can additionally be recovered from the redox material in the reactor, the temperature swing approach is preferred over isothermal operation [64]. However, solid-state heat recovery is highly challenging and no well-developed techniques for high-temperature operation exist yet [46,60,64–66].

2.4. Materials for Two-Step Thermochemical Water Splitting

Different redox materials were tested by various researchers in order to obtain a better understanding of the two-step thermochemical water splitting reaction, as well as to reduce the reduction temperature and to investigate the potential of producing hydrogen via this route. A rough distinction between volatile and non-volatile redox materials can be made. The performance of the materials could be improved, for example by doping and supporting metal (nano)structures.

Perovskites and poly-cation oxides have also been investigated for two-step thermochemical water splitting. Compared to the current state-of-the-art materials, modified ceria and ferrites, perovskites generally form more oxygen vacancies and are more easily reduced [67–69]. Poly-cation oxides were also recently investigated and compared to ceria and ferrites, and it was found that a higher hydrogen yield can be obtained, meaning that reduction can take place at a lower temperature [29,70]. Herein, we only discuss the materials based on ceria and ferrites, because these are currently considered state-of-the-art materials for thermochemical water splitting [29,71,72].

2.4.1. Volatile and Non-Volatile Redox Materials

Volatile redox materials become gaseous when the redox cycle is carried out, as the name suggests, due to the high temperature required for the reduction reaction. The main disadvantage of this is that gas quenching is necessary to separate the gaseous product and the redox material. The latter should then be reinjected into the reactor, otherwise it cannot be fully regenerated in the oxidation reaction and the produced hydrogen is contaminated. As a consequence, the productivity drops and the material often requires replacement. Examples of volatile redox materials for the two-step water splitting reaction include the MgO/Mg [73], ZnO/Zn and the SnO_2/SnO cycles [36,38,42,44,74].

Not all redox materials become gaseous during the two-step water splitting reaction, which are denoted as non-volatile redox materials, for which quenching is not needed. Therefore, these materials are often preferred over volatile materials, and more research has been performed on these materials. Examples of non-volatile redox materials are ceria and ferrite [36,38,42,74]. The ceria cycle especially has been found to be very promising due to the fast kinetics [35,75], which is mainly caused by the large number of oxygen vacancies generated during reduction of the redox material [3,76] due to the cubic fluorite crystal structure [77]. It has been noted that this crystal structure can form a maximum theoretical amount of eight oxygen vacancies per unit cell. This is higher than for the rock salt and zinc blended structure [78,79], where a maximum theoretical amount of four oxygen vacancies per unit cell can be formed.

Figure 10 shows a comparison of the maximum theoretical hydrogen yields under standard conditions based on the redox limit for two volatile (ZnO and SnO_2) and two non-volatile (CeO_2 and Fe_2O_3) redox materials. As seen in the figure, higher hydrogen yields are obtained for volatile materials, which is their main advantage over non-volatile redox materials. Still, their cycle efficiency is very low due to the required quenching [38,80,81]. Hence, it is desirable to focus on improving the hydrogen yields of non-volatile redox materials.

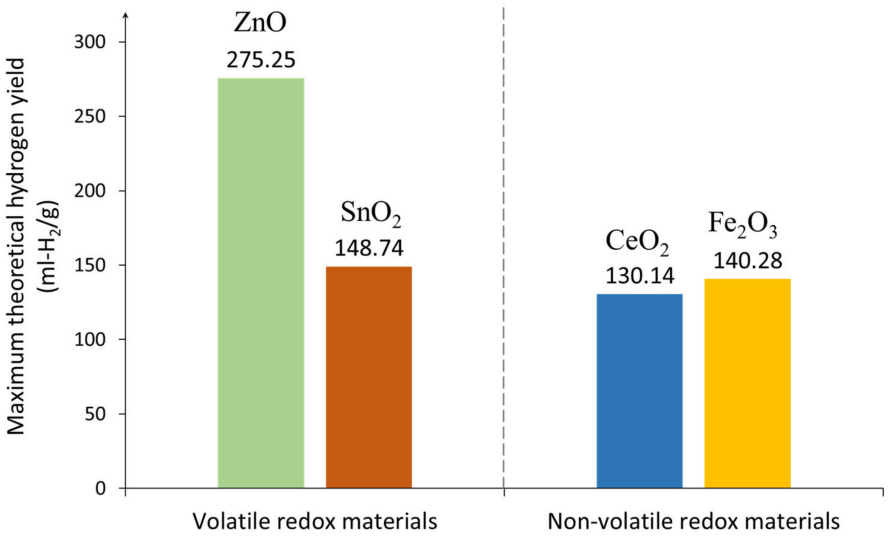

Figure 10. Comparison of the maximum theoretical hydrogen yields under standard conditions, calculated based on the redox limits for the volatile redox materials ZnO and SnO_2 and the non-volatile redox materials CeO_2 and Fe_2O_3. Redrawn from [38].

2.4.2. Improvements of the Performance of Non-Volatile Redox Materials

Several methods to improve the performance of non-volatile redox materials have been experimentally tested over the years, and the main goals of these experiments were to run the reduction reaction at a lower temperature, to reduce the cycling time, to mitigate sintering and to maintain a reasonable hydrogen yield or to increase it.

Doping the redox material can lead to higher mobility of the oxygen vacancies [74,82,83] and allows for a lower reduction in temperature [84], either via the formation of more oxygen vacancies or by having the oxygen sites closer to each other. In the first case, the metal in the undoped redox material is partly replaced by a metal with a smaller ionic radius, while in the second case the metal is partly substituted by a metal with a lower valency [74]. Doping ceria with zirconium has been shown to successfully enhance the mobility of oxygen vacancies, and a higher hydrogen yield can be achieved when more zirconium is added. Compared to undoped ceria, the same hydrogen yield can be achieved at a lower reduction temperature when zirconium is added. The thermal stability is also improved, and isothermal operation has been proven to be possible [36,38,74,85]. The hydrogen yields from isothermal cycling as a function of temperature are shown in Figure 11 for different zirconium contents, where is can be seen that an optimum level is reached when 15% to 20% of the cerium is substituted by zirconium. Next to zirconium, ceria can be doped by samarium, which induces stable hydrogen yields over multiple cycles [38,86] and reduces the reduction temperature [36]. The values reported in Figure 11 are lower compared to what is shown in Figure 10. Whereas Figure 10 shows the calculated maximum theoretical hydrogen production, the graph shown in Figure 11 was obtained from experimental results. Differences in hydrogen production are expected when varying the operating conditions, with assumptions being made to calculate the values reported in Figure 10 and non-ideal behavior when testing real materials.

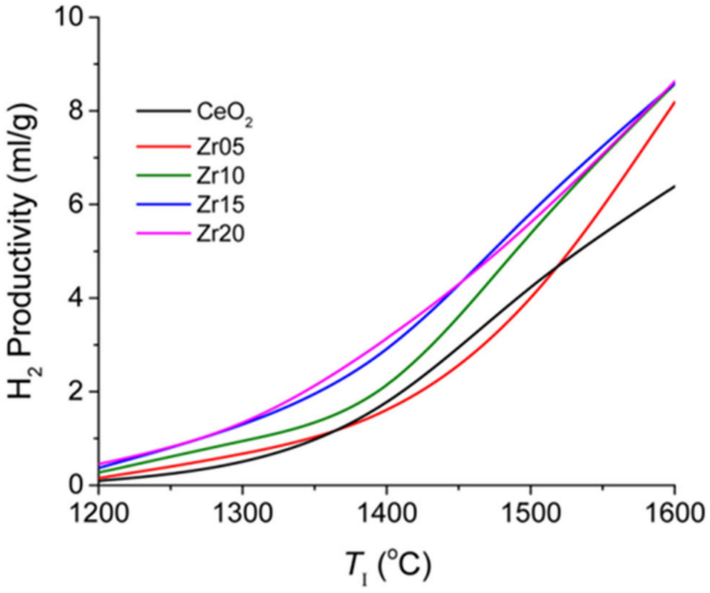

Figure 11. Hydrogen yields for isothermal two-step thermochemical water splitting at different doping concentrations of zirconium in cerium oxide, including cerium (IV) oxide without doping. Reprinted from [85].

The computational investigation revealed that the reduction energy is lowered for zirconium-doped ceria as the energy stored in strained Zr-O bonds is released when oxygen vacancies are formed [87]. From atomistic simulations, it was concluded that the oxygen vacancies are usually formed next to zirconium, which has been confirmed in two computational studies [85]. The first study attributed this finding to the small zirconium ion, which prefers 7-fold oxygen coordination over a coordination number of 8. The 7-fold coordination can be accommodated in reduced ceria [85,88]. The second study reported that the binding between oxygen vacancies and tetravalent ions is favorable for decreasing ionic radii, such that it is more energetically favorable to form oxygen vacancies near the zirconium ion instead of the cerium ion [85,89].

It has often been found for multiple redox materials that the hydrogen production tends to decrease with the number of cycles due to deactivation of the material. A major cause of deactivation in the two-step thermochemical water splitting reaction is sintering, since the reactions are operated at high temperatures [36,83]. Sintering has especially been found to be a major problem for the (unsupported) Fe_3O_4/FeO-cycle [30,38,44,50,74,90]. Another challenge with ferrites is the formation of an oxide layer, which leads to a reduction in the active surface area, such that the hydrogen generation drops significantly [35,45,91]. The reducing temperature of Fe_3O_4 can be lowered by partially substituting the iron ions with other metals, for example manganese or nickel [30,35,42,45,50], with nickel ferrites especially showing promising results, as it was shown that the hydrogen yield increased and was stable over multiple cycles [38].

Supports could solve some of the challenges related with unsupported materials, as discussed above. For example, when Fe_3O_4 is supported on yttrium-stabilized zirconia [30,92] or monoclinic zirconium (IV) oxide [30,93], sintering is alleviated. The results for Fe_3O_4 supported on yttrium-stabilized zirconia were found to be more promising compared to the redox material supported on monoclinic zirconium (IV) oxide [30]. When Fe_3O_4 is supported on yttrium-stabilized zirconia, the hydrogen yield is approximately constant, as also shown in Figure 12.

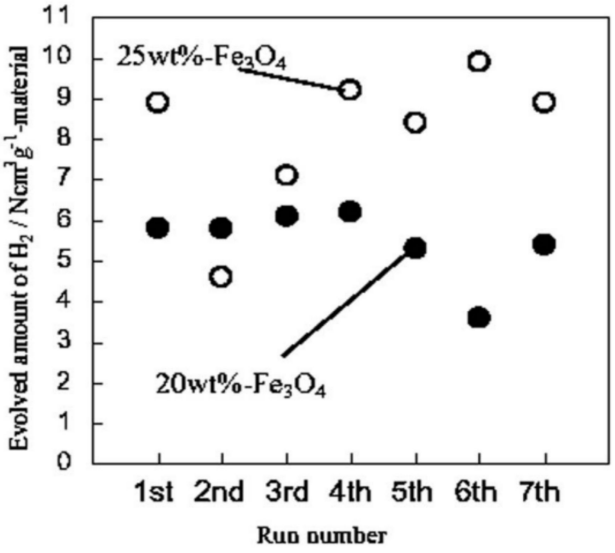

Figure 12. Evolved amount of hydrogen as a function of the run number for Fe_3O_4 supported on yttrium-stabilized zirconia. The reduction temperature was 1400 °C. The solid circles represent 20 wt%-Fe_3O_4 and the open circles represent 25 wt%-Fe_3O_4. Reprinted from [30].

Supporting Fe_3O_4 or manganese ferrite on zirconium (IV) oxide also results in less sintering [35], as well as increased reduction rates, a higher yield for the former and improved cyclability for the latter. When nickel ferrites are supported on (monoclinic) zirconium (IV) oxide, the reactivity is improved, which is possibly caused by the alleviation of sintering [50] and a combination of the formation of more oxygen vacancies and increased mobility of these vacancies [38]. The cyclability of the material was, thus, improved compared to unsupported ferrites [50], as can also be seen in Figure 13, which shows that the amounts of hydrogen generated are approximately constant over multiple cycles. This relatively constant hydrogen production over multiple cycles would not be seen with sintering. It is also shown in Figure 13 that the performance of the material is further improved when the ferrites are also doped with nickel.

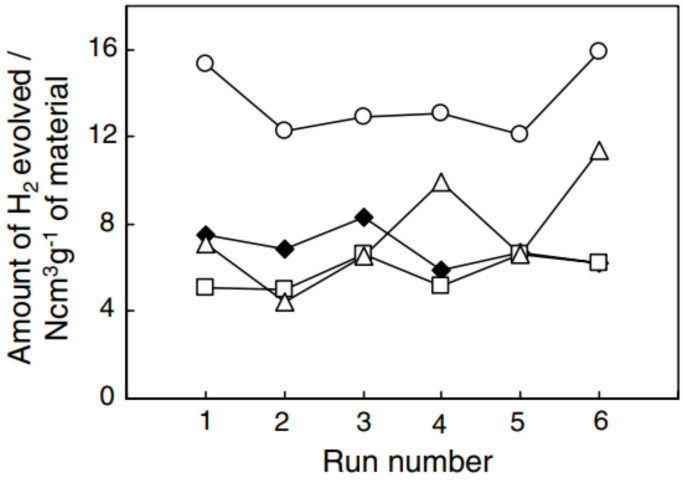

Figure 13. Amount of hydrogen generated as a function of the cycle number. The reduction reaction took place at 1400 °C. The open circles represent $NiFe_2O_4$/m-ZrO_2, the open triangles $Ni_{0.65}Fe_{2.35}O_4$/m-ZrO_2, the diamonds Fe_3O_4/m-ZrO_2 and the open squares $Ni_{0.35}Fe_{2.65}O_4$/m-ZrO_2. Monoclinic zirconium (IV) oxide is denoted by m-ZrO_2 in this figure and the ferrite loading on the support was 20 wt%. Reprinted from [50].

The operating conditions for testing the materials as shown in Figures 12 and 13 were almost identical; only the flowrate for oxidation, reduction time and oxidation time differed. The materials shown in Figure 12 were reduced for 1 h and oxidized for 50 min. For oxidation, the flowrate of nitrogen bubbled through water was 3 N cm^3/min [30]. The reduction and oxidation time were 30 min and 1 h, respectively, for the materials shown in Figure 13. Nitrogen was bubbled through water at a flowrate of 4 N cm^3/min during the oxidation reaction [50]. Comparing the results reported in Figure 12 for 20 wt% loading of Fe_3O_4 to those in Figure 13, once can see that the difference in hydrogen production over multiple cycles is similar for ferrites supported on yttrium-stabilized zirconia and monoclinic zirconium (IV) oxide. The hydrogen production increases with increasing nickel-dopant concentration, as shown in Figure 13. Compared to 25 wt% loading of Fe_3O_4 on yttrium-stabilized zirconia, the hydrogen production of $NiFe_2O_4$ supported on monoclinic zirconium (IV) oxide is improved.

Oxide supports are frequently used to improve particle dispersion and stability. Regarding supporting materials suitable for this application, a large surface area combined with good thermal stability is desirable due to the reactions taking place at elevated temperatures, such as γ-Al_2O_3. Combining this oxide with rhodium further improves the thermal stability because of the strong interactions between them. The combination of rhodium with γ-Al_2O_3 for ceria has been experimentally tested, where it was shown that although the thermal stability was improved, sintering and the formation of cerium-aluminum oxides at higher temperatures still lead to lower hydrogen yields. The hydrogen production has been shown to be unstable over multiple cycles, especially for oxidation at temperatures as high as 1200 °C. The feed for this process was a water-ethanol mixture, such that the hydrogen production was increased due to the high hydrogen content of ethanol [3]. When only rhodium is added to ceria, the cycling times are reduced during isothermal operation, as also seen in Figure 14 [64].

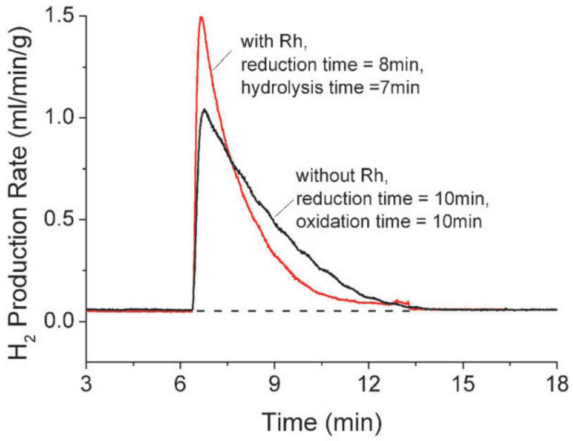

Figure 14. Effects of rhodium added to cerium (IV) oxide on the reduction and oxidation times, as well as on the hydrogen production rate during isothermal cycling at a temperature of 1500 °C. Reprinted from [64].

Decreasing the particle size of the redox materials has been shown to positively influence reactivity. The reason for this is the reduction in diffusion length [35,42,45,74,85], as well as the continuous entrainment of the particles by gas [35,45,94]. However, it has also been shown that a very fine powder is not desired, as it will sinter easily and form a dense mass [85,95,96], leading to reduced hydrogen production.

In order to increase the surface area, ceria core nanowires with a tin (IV) oxide shell around it were synthesized on a porous nickel foam disk. It was found that more hydrogen was produced compared to a thin film of ceria and that no substantial reduction in surface area was observed after multiple cycles [2], indicating good cyclability. The use of different

ordered materials has been proposed to improve the results from undoped and unsupported ceria [74,97–99].

Ceria has also been synthesized using cork templates, and good cyclability together with a drastically increased hydrogen generation rate were found. The cork came from Mediterranean evergreen oak bark, which has been found to exhibit a 3D ordered macroporous cellular microstructure [42]. The authors were able to use cork granules as a hard template to obtain 3D-ordered ceria through an impregnation process. The increased hydrogen production rate may be partly explained by the increased surface area. The results from this material were better than for ceria foams, which can be explained by the highly ordered structure obtained from the cork templates, because the structure allows for controlled transport of the reactants towards the active sites [42,100,101]. In practice, the structure of foams is usually random [102], so transport is hampered compared to with an ordered structure [99].

Another method that has been researched to obtain stable hydrogen yield over multiple cycles involves encapsulating a nickel ferrite nanoparticle core in an yttrium (III) oxide shell. The hydrogen yield was shown to be approximately constant over at least five cycles, possibly due to the lower level of sintering because of the ceramic shell. In Figure 15, the hydrogen production rate over time is plotted, showing five cycles. A comparison between the core–shell nanoparticles, the powder and the nanoparticles without a shell is also shown, and it can be seen that the core–shell nanoparticles improve the cyclability compared to the other configurations. It can also be seen that the amount of hydrogen produced is lower for the core-shell nanoparticles compared to the amount produced by the nickel ferrite nanoparticles or the powdered mixture consisting of nickel ferrite and yttrium (III) oxide [103]. The reduced yield may be caused by the ceramic shell inducing mass transfer limitations [103–105].

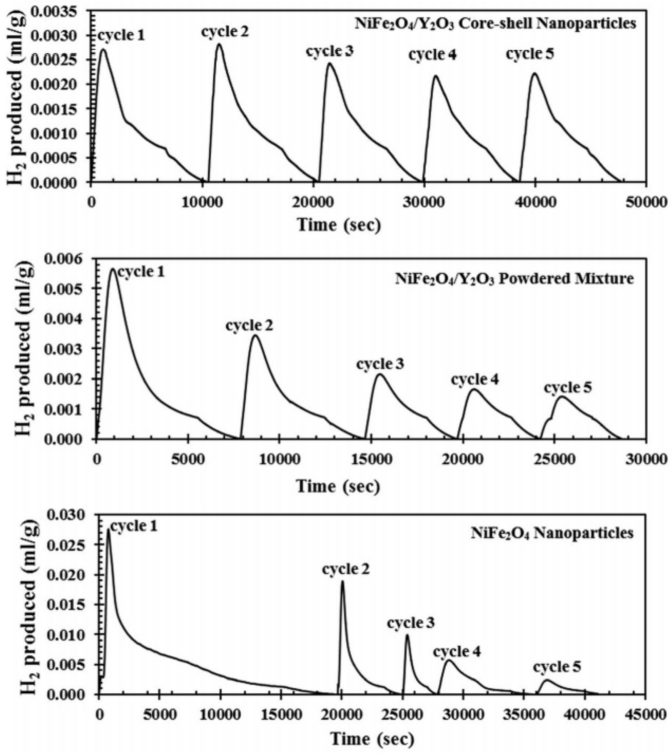

Figure 15. Hydrogen production rate in mL/s/g over time, showing five redox cycles for nanoparticles with a nickel ferrite core and an yttrium (III) oxide shell and a powdered mixture including nickel ferrite and yttrium (III) oxide and nickel ferrite nanoparticles. Reprinted from [103].

2.4.3. Multi-Criteria Analysis of Non-Volatile Redox Materials

A comparison between several promising non-volatile redox materials was performed using a multi-criteria analysis, as shown in Figure 16. Several criteria were defined together with their weights, with 1 indicating not important and 5 indicating very important. The scores for the different materials ranged between 1 and 5, with 1 being very bad and 5 being very good. If information for a criterion was found in the literature, the cell in the table was colored grey and an estimation was made if possible. For example, it was found that ferrites generally are accompanied by long cycling times, but when an estimation could not be made, the number 3 (meaning indifferent) was filled in. When redox materials were discussed in multiple reports, the scores were defined for each article and then the average was determined and provided in the table.

Multi-criteria analysis											
		Cerium oxides						Iron oxides			
Criteria	**Weight**	**1**	**2**	**3**	**4**	**5**	**6**	**7**	**8**	**9**	**10**
Little sintering	4	4	3	3	4	4	3	3	4	4	4
Small temperature difference between reactions (< 150 °C)	3	3	3	5	2	2	2	2	2	2	3
High hydrogen generation (> 0.2 L hydrogen/g·cycle)	3	2	2	2	4	5	1	2	2	2	2
Stable hydrogen yield	4	3	3	3	4	4	4	4	4	4	4
Stable material	4	4	4	3	4	3	2	4	4	3	3
Short cycle time (< 10 min)	2	2	4	4	3	2	2	2	2	2	2
Total		63	63	65	72	69	49	60	64	60	63
1	Doped with zirconium										
2	Doped with samarium										
3	Rhodium addition										
4	Rhodium addition and supported on γ-Al_2O_3										
5	Core nano-wires with a tin(IV) oxide shell on a porous nickel foam disk										
6	Using cork-templates										
7	Doped with nickel										
8	Supported on yttrium-stabilized zirconia										
9	Doped with nickel and supported on monoclinic zirconium(IV) oxide										
10	Doped with nickel core with a yttrium(III) oxide shell										

Figure 16. Multi-criteria analysis including the criteria and weights of the redox materials suitable for thermochemical two-step water splitting.

According to this analysis, ceria with rhodium supported on γ-Al_2O_3 seems to be the most promising. However, a large error margin should be taken into account when a multi-criteria analysis is used for selection, as all numbers are relative. Therefore, it could also be stated that nanowires with a ceria core and a tin (IV) oxide shell on a porous nickel foam disk, ceria with rhodium, iron oxides supported on yttrium-stabilized zirconia, ceria doped with zirconia or samarium and iron oxide doped with a nickel core and an yttrium (III) oxide shell are also promising approaches at this point, with the last three materials having the same total score.

Table 2 contains all of the examined materials with the relative hydrogen production rates and total amounts of hydrogen per cycle. The reaction conditions and oxidation temperatures are also included. It is possible to notice that not all the data were obtained under similar experimental conditions, so it is quite difficult to make a reliable comparison.

Table 2. Multi-criteria analysis including the criteria and weights of the redox materials suitable for thermochemical two-step water splitting.

Number on the Multi-Criteria Analysis	Redox Material	Reduction Temperature (°C)	Oxidation Temperature (°C)	Maximum H_2 Production Rate ($mL \cdot g^{-1} \cdot min^{-1}$)	H_2 Production on a Single Cycle ($mL \cdot g^{-1}$)	Ref.
1	$Ce_{0.75}Zr_{0.25}O_2$	1450	1045	0.47	5.33	[38,74]
2	$Ce_{1-x}Sm_xO_2$	1500	900	4.1	3.8	[38,86]
3	Rh/CeO_2	1500	1500	1.5	n.a.	[64]
4	$Rh/CeO_2/\gamma$-Al_2O_3	1050	1200	n.a.	1424.5	[3]
5	CeO_2/SnO_2 core-shell nanowires	Reduced material obtained after CeO_2 pulse laser deposition	800	2.14	720.4 mL per gram of CeO_2 (not referred to total material)	[2]
6	cork-templated CeO_2	1450	1050	1.6	3.83	[42]
7	$Ni_xFe_{3-x}O_4$	1400	1000	n.a.	11	[38,50]
		1450	1000	0.314	14.11	[38,106]
8	Fe_3O_4 on yttrium-stabilized, cubic zirconia (YSZ)	1400	1000	0.5	9	[30]
9	$Ni_xFe_{3-x}O_4$ supported on ZrO_2	1400	1000	0.65	15	[50]
10	$NiFe_2O_4/Y_2O_3$ core-shell nanoparticles	1100	900	0.162	10.39	[103]

3. Conclusions, Current Challenges and Future Directions

Thermochemical water splitting using redox cycles has potential for sustainable hydrogen production. By employing non-volatile redox materials, it is possible to avoid the quenching required for thermochemical cycling with volatile redox materials. This was found to be a major advantage of non-volatile materials, such as CeO_2, over volatile materials, such as ZnO and SnO_2.

The thermodynamic analysis showed that the reaction can be driven forward using either a temperature swing or a pressure swing approach. The main challenges encountered using a temperature swing during operation are related to the fact that the process is energy-intensive. The pressure swing operation would be highly desirable, as this allows for isothermal cycling. Considering the advantages and disadvantages of both temperature looping and the pressure swing, it might be desired to operate nearly isothermally, such that the advantages of the pressure swing approach are utilized with an additional driving force in the form of a small temperature difference. It is expected that the minor temperature swing would not suppress the advantages of the pressure swing, while it would have the major advantage of the temperature swing approach. This was also suggested by Muhich et al. [63].

The reactors described in this report are mainly suitable for non-volatile redox materials. The technology used to concentrate solar light is already well-established and allows for operation at temperatures up to 2000 °C, which is favorable for the reduction reaction. However, the oxidation reaction is favored at lower temperatures [31]. In order to obtain reasonable hydrogen yields using a solar reactor, the temperature needs to be heavily decreased, although with solar reactors this cooling action is slow. Moreover, the availability and intensity of the sunlight differ in various regions, which could also limit the

widespread adoption of solar light-based reactors. Using an electrically powered furnace could be an interesting option, provided that the electricity is produced from renewable sources. Moreover, in such furnaces, extremely high temperatures equal to those seen in solar reactors cannot be reached, although the oxidation temperatures can be obtained faster and a reasonable amount of hydrogen is still produced. Hence, a system where the samples can be heated and cooled fast is highly desirable. As described above, this is one of the main features of microwave-oven-based systems, although it is necessary to overcome the technical challenges in microwave oven use. An interesting option could be to develop a reactor with two zones, one where the material can be heated fast, after which it is transported to a cool region similar to a fluidized bed reactor to avoid the heating–cooling cycles.

In terms of redox material development, volatile redox materials have higher theoretical hydrogen yields compared to non-volatile redox materials, as seen in Figure 10. Although this is a major advantage of volatile materials over non-volatile materials, the quenching of the material is a major bottleneck, and a trade-off has to be made. From a research perspective, it would be advisable to predominantly focus on non-volatile redox materials to obtain a better understanding of how the materials in the system behave, without losing material during cycling due to volatility. A highly interesting approach could be to incorporate the properties of volatile materials into non-volatile materials. The most promising materials shown in Figure 16 should be investigated further.

A well-known challenge with the current materials is the decrease in hydrogen yields over multiple cycles due to sintering. Figures 12 and 13 show relatively constant hydrogen production. Therefore, one could look into the workings of the nickel dopant and the yttrium-stabilized zirconia and (monoclinic) zirconium (IV) oxide supports. Another strategy could be the use of a core–shell structure. As shown in Figure 15, the core–shell nanoparticles show approximately constant hydrogen yields over multiple cycles. However, the shell provides a mass transport barrier, such that the hydrogen yield is low compared to other materials. Core–shell nanoparticles with a thinner shell could provide more hydrogen per cycle. The hydrogen yields could possibly be further improved by using a volatile core with a non-volatile shell around it. The shell could form a mass transport barrier, which would keep the volatile matter inside the core, where it should recombine into the original composition. Although the shell should be of sufficient thickness to keep the volatile components in the core, it should not be too thick in order to allow for reactants and products to penetrate through the shell and to produce a reasonable amount of hydrogen. Instead of altering the shell thickness, the pore size of the shell could be varied. As oxygen, hydrogen and water are relatively small molecules compared to metal oxides, adjusting the pore size such that only product gases and water can pass through the shell would be the ideal solution.

Other common methods used to improve conventional non-volatile redox materials, such as ceria and ferrite, are doping, the addition of ceramic supports and decreasing the size of the enhanced surface areas through the use of nanosized particles or structures. The use of ordered structures, such as nanowires or cork templates, has led to higher hydrogen production rates, possibly due to enhanced mass transfer to and from the oxygen vacancies as a pre-defined path is constructed.

In situ spectroscopic studies would be interesting to include in future research to reveal the formation of oxygen vacancies during the reduction reaction and the subsequent hydrogen generation while the redox material is being oxidized, because this is expected to assist in the development of novel materials and their ordering for thermochemical water splitting for hydrogen generation.

Author Contributions: Conceptualization, A.B. and D.O.; Writing—original draft preparation, D.O. and M.O.; supervision, A.B.; writing—review and editing, A.B., A.C., N.D. and S.A.; validation, A.B., N.D., A.C. and S.A. All authors have read and agreed to the published version of the manuscript.

Funding: This work was supported in part by TU Delft Process & Product Technology Institute (*Pro2Tech, formerly DPTI*) via DPTI 2021 award to A.B. The research stay of M.O. was funded by Toso Montanari Foundation, University of Bologna, Italy.

Institutional Review Board Statement: Not applicable.

Informed Consent Statement: Not applicable.

Data Availability Statement: Not applicable.

Conflicts of Interest: The authors declare no conflict of interest.

References

1. Goelzer, H.; Nowicki, S.; Payne, A.; Larour, E.; Seroussi, H.; Lipscomb, W.H.; Gregory, J.; Abe-Ouchi, A.; Shepherd, A.; Simon, E.; et al. The future sea-level contribution of the Greenland ice sheet: A multi-model ensemble study of ISMIP6. *Cryosphere* **2020**, *14*, 3071–3096. [CrossRef]
2. Seo, K.; Lim, T.; Mills, E.M.; Kim, S.; Ju, S. Hydrogen generation enhanced by nano-forest structures. *RSC Adv.* **2016**, *6*, 12953–12958. [CrossRef]
3. Roychowdhury, S.; Mukthar Ali, M.; Dhua, S.; Sundararajan, T.; Ranga Rao, G. Thermochemical hydrogen production using Rh/CeO2/γ-Al2O3 catalyst by steam reforming of ethanol and water splitting in a packed bed reactor. *Int. J. Hydrogen Energy* **2021**, *46*, 19254–19269. [CrossRef]
4. Safari, F.; Dincer, I. A review and comparative evaluation of thermochemical water splitting cycles for hydrogen production. *Energy Convers. Manag.* **2020**, *205*, 112182. [CrossRef]
5. Dundar-Tekkaya, E.; Yürüm, Y. Mesoporous MCM-41 material for hydrogen storage: A short review. *Int. J. Hydrogen Energy* **2016**, *41*, 9789–9795. [CrossRef]
6. Luo, Q.-H.; Hu, J.-B.; Sun, B.-G.; Liu, F.-S.; Wang, X.; Li, C.; Bao, L.-Z. Experimental investigation of combustion characteristics and NOx emission of a turbocharged hydrogen internal combustion engine. *Int. J. Hydrogen Energy* **2019**, *44*, 5573–5584. [CrossRef]
7. Ciniviz, M.; Köse, H. Hydrogen Use in Internal Combustion Engine: A Review. *Int. J. Automot. Eng. Technol.* **2012**, *1*, 1–15.
8. White, C.M.; Steeper, R.R.; Lutz, A.E. The hydrogen-fueled internal combustion engine: A technical review. *Int. J. Hydrogen Energy* **2006**, *31*, 1292–1305. [CrossRef]
9. Kulkarni, T.; Slaughter, G. Enzymatic Glucose Biofuel Cell and its Application. *J. Biochips Tissue Chips* **2015**, *5*, 1000111.
10. Tuan, K.N.; Karpukhin, K.E.; Terenchenko, A.S.; Kolbasov, A.F. World trends in the development of vehicles with alternative energy sources. *ARPN J. Eng. Appl. Sci.* **2018**, *13*, 2535–2542.
11. Acar, C.; Dincer, I. 3.1 Hydrogen Production. In *Comprehensive Energy Systems*; Dincer, I., Ed.; Elsevier: Oxford, UK, 2018; pp. 1–40.
12. Dawood, F.; Anda, M.; Shafiullah, G.M. Hydrogen production for energy: An overview. *Int. J. Hydrogen Energy* **2020**, *45*, 3847–3869. [CrossRef]
13. Kakoulaki, G.; Kougias, I.; Taylor, N.; Dolci, F.; Moya, J.; Jäger-Waldau, A. Green hydrogen in Europe—A regional assessment: Substituting existing production with electrolysis powered by renewables. *Energy Convers. Manag.* **2021**, *228*, 113649. [CrossRef]
14. LeValley, T.L.; Richard, A.R.; Fan, M. The progress in water gas shift and steam reforming hydrogen production technologies—A review. *Int. J. Hydrogen Energy* **2014**, *39*, 16983–17000. [CrossRef]
15. Acar, C.; Dincer, I. Comparative assessment of hydrogen production methods from renewable and non-renewable sources. *Int. J. Hydrogen Energy* **2014**, *39*, 1–12. [CrossRef]
16. Acar, C.; Dincer, I. Review and evaluation of hydrogen production options for better environment. *J. Clean. Prod.* **2019**, *218*, 835–849. [CrossRef]
17. Detchusananard, T.; Im-orb, K.; Ponpesh, P.; Arpornwichanop, A. Biomass gasification integrated with CO_2 capture processes for high-purity hydrogen production: Process performance and energy analysis. *Energy Convers. Manag.* **2018**, *171*, 1560–1572. [CrossRef]
18. Shiva Kumar, S.; Himabindu, V. Hydrogen production by PEM water electrolysis—A review. *Mater. Sci. Energy Technol.* **2019**, *2*, 442–454. [CrossRef]
19. Zhang, K.; Ma, M.; Li, P.; Wang, D.H.; Park, J.H. Water Splitting Progress in Tandem Devices: Moving Photolysis beyond Electrolysis. *Adv. Energy Mater.* **2016**, *6*, 1600602. [CrossRef]
20. Singh, R.; Dutta, S. A review on H_2 production through photocatalytic reactions using TiO_2/TiO_2-assisted catalysts. *Fuel* **2018**, *220*, 607–620. [CrossRef]
21. Ayers, K.; Anderson, E.; Capuano, C.; Carter, B.; Dalton, L.; Hanlon, G.; Manco, J.; Niedzwiecki, M. Research Advances Towards Low Cost, High Efficiency PEM Electrolysis. *ECS Trans.* **2010**, *33*, 3. [CrossRef]
22. Lee, J.E.; Shafiq, I.; Hussain, M.; Lam, S.S.; Rhee, G.H.; Park, Y.-K. A review on integrated thermochemical hydrogen production from water. *Int. J. Hydrogen Energy* **2022**, *47*, 4346–4356. [CrossRef]
23. Funk, J.E.; Conger, W.L.; Carty, R.H. Evaluation of Multi-Step Thermochemical Processes for the Production of Hydrogen from Water. In *Hydrogen Energy*; Springer: Boston, MA, USA, 1975.
24. Jansen, G.; Dehouche, Z.; Corrigan, H. Cost-effective sizing of a hybrid Regenerative Hydrogen Fuel Cell energy storage system for remote & off-grid telecom towers. *Int. J. Hydrogen Energy* **2021**, *46*, 18153–18166.

25. Abanades, S. Metal Oxides Applied to Thermochemical Water-Splitting for Hydrogen Production Using Concentrated Solar Energy. *ChemEngineering* **2019**, *3*, 63. [CrossRef]
26. Xiao, L.; Wu, S.-Y.; Li, Y.-R. Advances in solar hydrogen production via two-step water-splitting thermochemical cycles based on metal redox reactions. *Renew. Energy* **2012**, *41*, 1–12. [CrossRef]
27. Ohta, T. Chapter 4—Direct Thermal Decomposition of Water. In *Solar-Hydrogen Energy Systems*; Pergamon: Oxford, UK, 1979; pp. 59–79.
28. Lorentzou, S.; Pagkoura, C.; Zygogianni, A.; Karagiannakis, G.; Konstandopoulos, A.G. Thermochemical cycles over redox structured reactors. *Int. J. Hydrogen Energy* **2017**, *42*, 19664–19682. [CrossRef]
29. Zhai, S.; Rojas, J.; Ahlborg, N.; Lim, K.; Toney, M.F.; Jin, H.; Chueh, W.C.; Majumdar, A. The use of poly-cation oxides to lower the temperature of two-step thermochemical water splitting. *Energy Environ. Sci.* **2018**, *11*, 2172–2178. [CrossRef]
30. Kodama, T.; Nakamuro, Y.; Mizuno, T. A Two-Step Thermochemical Water Splitting by Iron-Oxide on Stabilized Zirconia. *J. Sol. Energy Eng.* **2004**, *128*, 3–7. [CrossRef]
31. Muhich, C.; Evanko, B.; Weston, K.; Lichty, P.; Liang, X.; Martinek, J.; Musgrave, C.; Weimer, A. Efficient Generation of H-2 by Splitting Water with an Isothermal Redox Cycle. *Science* **2013**, *341*, 540–542. [CrossRef]
32. Le Gal, A.; Abanades, S. Dopant Incorporation in Ceria for Enhanced Water-Splitting Activity during Solar Thermochemical Hydrogen Generation. *J. Phys. Chem. C* **2012**, *116*, 13516–13523. [CrossRef]
33. Han, S.B.; Kang, T.B.; Joo, O.S.; Jung, K.D. Water splitting for hydrogen production with ferrites. *Sol. Energy* **2007**, *81*, 623–628. [CrossRef]
34. Bhosale, R.R. Solar hydrogen production via thermochemical magnesium oxide—Magnesium sulfate water splitting cycle. *Fuel* **2020**, *275*, 117892. [CrossRef]
35. Abanades, S.; Flamant, G. Thermochemical hydrogen production from a two-step solar-driven water-splitting cycle based on cerium oxides. *Sol. Energy* **2006**, *80*, 1611–1623. [CrossRef]
36. Le Gal, A.; Abanades, S.; Bion, N.; Le Mercier, T.; Harlé, V. Reactivity of Doped Ceria-Based Mixed Oxides for Solar Thermochemical Hydrogen Generation via Two-Step Water-Splitting Cycles. *Energy Fuels* **2013**, *27*, 6068–6078. [CrossRef]
37. Tamaura, Y.; Steinfeld, A.; Kuhn, P.; Ehrensberger, K. Production of solar hydrogen by a novel, 2-step, water-splitting thermochemical cycle. *Energy* **1995**, *20*, 325–330. [CrossRef]
38. Mao, Y.; Gao, Y.; Dong, W.; Wu, H.; Song, Z.; Zhao, X.; Sun, J.; Wang, W. Hydrogen production via a two-step water splitting thermochemical cycle based on metal oxide—A review. *Appl. Energy* **2020**, *267*, 114860. [CrossRef]
39. Steinfeld, A. Solar thermochemical production of hydrogen—-A review. *Sol. Energy* **2005**, *78*, 603–615. [CrossRef]
40. Haeussler, A.; Abanades, S.; Jouannaux, J.; Julbe, A. Non-Stoichiometric Redox Active Perovskite Materials for Solar Thermochemical Fuel Production: A Review. *Catalysts* **2018**, *8*, 611. [CrossRef]
41. Gorensek, M.B.; Corgnale, C.; Staser, J.A.; Weidner, J.W. Chapter 3—Thermochemical Hydrogen Processes. In *Electrochemical Power Sources: Fundamentals, Systems, and Applications*; Smolinka, T., Garche, J., Eds.; Elsevier: Amsterdam, The Netherlands, 2022; pp. 63–82.
42. Costa Oliveira, F.A.; Barreiros, M.A.; Haeussler, A.; Caetano, A.P.F.; Mouquinho, A.I.; Oliveira e Silva, P.M.; Novais, R.M.; Pullar, R.C.; Abanades, S. High performance cork-templated ceria for solar thermochemical hydrogen production via two-step water-splitting cycles. *Sustain. Energy Fuels* **2020**, *4*, 3077–3089. [CrossRef]
43. Arribas, L.; Gonzalez-Aguilar, J.; Romero, M. Solar-Driven Thermochemical Water-Splitting by Cerium Oxide: Determination of Operational Conditions in a Directly Irradiated Fixed Bed Reactor. *Energies* **2018**, *11*, 2451. [CrossRef]
44. Chueh, W.; Falter, C.; Abbott, M.; Scipio, D.; Furler, P.; Haile, S.; Steinfeld, A. High-Flux Solar-Driven Thermochemical Dissociation of CO_2 and H_2O Using Nonstoichiometric Ceria. *Science* **2010**, *330*, 1797–1801. [CrossRef]
45. Charvin, P.; Abanades, S.; Flamant, G.; Lemort, F. Two-step water splitting thermochemical cycle based on iron oxide redox pair for solar hydrogen production. *Energy* **2007**, *32*, 1124–1133. [CrossRef]
46. Al-Shankiti, I.; Ehrhart, B.D.; Weimer, A.W. Isothermal redox for H_2O and CO_2 splitting—A review and perspective. *Sol. Energy* **2017**, *156*, 21–29. [CrossRef]
47. Martinek, J.; Viger, R.; Weimer, A.W. Transient simulation of a tubular packed bed solar receiver for hydrogen generation via metal oxide thermochemical cycles. *Sol. Energy* **2014**, *105*, 613–631. [CrossRef]
48. Kodama, T.; Gokon, N.; Matsubara, K.; Yoshida, K.; Koikari, S.; Nagase, Y.; Nakamura, K. Flux Measurement of a New Beam-down Solar Concentrating System in Miyazaki for Demonstration of Thermochemical Water Splitting Reactors. *Energy Procedia* **2014**, *49*, 1990–1998. [CrossRef]
49. Gokon, N.; Takahashi, S.; Yamamoto, H.; Kodama, T. Thermochemical two-step water-splitting reactor with internally circulating fluidized bed for thermal reduction of ferrite particles. *Int. J. Hydrogen Energy* **2008**, *33*, 2189–2199. [CrossRef]
50. Kodama, T.; Gokon, N.; Yamamoto, R. Thermochemical two-step water splitting by ZrO_2-supported $Ni_xFe_{3-x}O_4$ for solar hydrogen production. *Sol. Energy* **2008**, *82*, 73–79. [CrossRef]
51. Bhosale, R.; Shende, R.; Puszynski, J. H_2 Generation from Thermochemical Water-Splitting Using Sol-Gel Derived Ni-Ferrite. *J. Energy Power Eng.* **2010**, *4*, 27–38.
52. Bhosale, R.; Shende, R.; Puszynski, J. H_2 generation from thermochemical water-splitting using sol-gel synthesized ferrites ($M_xFe_yO_z$, M = Ni, Zn, Sn, Co, Mn, Ce). In Proceedings of the AIChE Annual Meeting, Salt Lake City, UT, USA, 7–12 November 2010.

53. Bhosale, R.; Khadka, R.; Puszynski, J.; Shende, R. H-2 generation from two-step thermochemical water-splitting reaction using sol-gel derived $Sn_xFe_yO_z$. *J. Renew. Sustain. Energy* **2011**, *3*, 063104. [CrossRef]
54. Bhosale, R.R.; Shende, R.V.; Puszynski, J.A. Thermochemical water-splitting for H_2 generation using sol-gel derived Mn-ferrite in a packed bed reactor. *Int. J. Hydrogen Energy* **2012**, *37*, 2924–2934. [CrossRef]
55. Gao, Y.; Mao, Y.; Song, Z.; Zhao, X.; Sun, J.; Wang, W.; Chen, G.; Chen, S. Efficient generation of hydrogen by two-step thermochemical cycles: Successive thermal reduction and water splitting reactions using equal-power microwave irradiation and a high entropy material. *Appl. Energy* **2020**, *279*, 115777. [CrossRef]
56. Gedye, R.; Rank, W.; Westaway, K. The rapid synthesis of organic compounds in microwave ovens. II. *Can. J. Chem.* **1991**, *69*, 706–711. [CrossRef]
57. Hoseinzadeh Hesas, R.; Wan Daud, W.M.A.; Sahu, J.N.; Arami-Niya, A. The effects of a microwave heating method on the production of activated carbon from agricultural waste: A review. *J. Anal. Appl. Pyrolysis* **2013**, *100*, 1–11. [CrossRef]
58. Roeb, M.; Sattler, C. Isothermal Water Splitting. *Science* **2013**, *341*, 470–471. [CrossRef] [PubMed]
59. Ganzoury, M.A.; Fateen, S.-E.K.; El Sheltawy, S.T.; Radwan, A.M.; Allam, N.K. Thermodynamic and efficiency analysis of solar thermochemical water splitting using Ce–Zr mixtures. *Sol. Energy* **2016**, *135*, 154–162. [CrossRef]
60. Felinks, J.; Brendelberger, S.; Roeb, M.; Sattler, C.; Pitz-Paal, R. Heat recovery concept for thermochemical processes using a solid heat transfer medium. *Appl. Therm. Eng.* **2014**, *73*, 1006–1013. [CrossRef]
61. Warren, K.J.; Tran, J.T.; Weimer, A.W. A thermochemical study of iron aluminate-based materials: A preferred class for isothermal water splitting. *Energy Environ. Sci.* **2022**, *15*, 806–821. [CrossRef]
62. Ermanoski, I.; Miller, J.E.; Allendorf, M.D. Efficiency maximization in solar-thermochemical fuel production: Challenging the concept of isothermal water splitting. *Phys. Chem. Chem. Phys.* **2014**, *16*, 8418–8427. [CrossRef]
63. Muhich, C.; Ehrhart, B.; Alshankiti, I.; Ward, B.; Musgrave, C.; Weimer, A. A review and perspective of efficient hydrogen generation via solar thermal water splitting: A review and perspective of efficient hydrogen generation. *WIREs Energy Environ.* **2015**, *5*, 261–287. [CrossRef]
64. Hao, Y.; Yang, C.-K.; Haile, S.M. High-temperature isothermal chemical cycling for solar-driven fuel production. *Phys. Chem. Chem. Phys.* **2013**, *15*, 17084–17092. [CrossRef]
65. Kong, H.; Hao, Y.; Jin, H. Isothermal versus two-temperature solar thermochemical fuel synthesis: A comparative study. *Appl. Energy* **2018**, *228*, 301–308. [CrossRef]
66. Brendelberger, S.; Felinks, J.; Roeb, M.; Sattler, C. Solid Phase Heat Recovery and Multi Chamber Reduction for Redox Cycles. In Proceedings of the ASME 2014 8th International Conference on Energy Sustainability Collocated with the ASME 2014 12th International Conference on Fuel Cell Science, Engineering and Technology, Boston, MA, USA, 30 June–2 July 2014.
67. Demont, A.; Abanades, S.; Beche, E. Investigation of Perovskite Structures as Oxygen-Exchange Redox Materials for Hydrogen Production from Thermochemical Two-Step Water-Splitting Cycles. *J. Phys. Chem. C* **2014**, *118*, 12682–12692. [CrossRef]
68. Yang, C.-K.; Yamazaki, Y.; Aydin, A.; Haile, S.M. Thermodynamic and kinetic assessments of strontium-doped lanthanum manganite perovskites for two-step thermochemical water splitting. *J. Mater. Chem. A* **2014**, *2*, 13612–13623. [CrossRef]
69. Rao, C.N.R.; Dey, S. Solar thermochemical splitting of water to generate hydrogen. *Proc. Natl. Acad. Sci. USA* **2017**, *114*, 13385–13393. [CrossRef] [PubMed]
70. Barcellos, D.R.; Sanders, M.D.; Tong, J.; McDaniel, A.H.; O'Hayre, R.P. $BaCe_{0.25}Mn_{0.75}O_{3-\delta}$—A promising perovskite-type oxide for solar thermochemical hydrogen production. *Energy Environ. Sci.* **2018**, *11*, 3256–3265. [CrossRef]
71. Budama, V.K.; Johnson, N.G.; Ermanoski, I.; Stechel, E.B. Techno-economic analysis of thermochemical water-splitting system for Co-production of hydrogen and electricity. *Int. J. Hydrogen Energy* **2021**, *46*, 1656–1670. [CrossRef]
72. Dimitrakis, D.; Tsongidis, N.; Konstandopoulos, A. Reduction enthalpy and charge distribution of substituted ferrites and doped ceria for thermochemical water and carbon dioxide splitting with DFT+U. *Phys. Chem. Chem. Phys.* **2016**, *18*, 23587–23595. [CrossRef]
73. Gálvez, M.E.; Frei, A.; Albisetti, G.; Lunardi, G.; Steinfeld, A. Solar hydrogen production via a two-step thermochemical process based on MgO/Mg redox reactions—Thermodynamic and kinetic analyses. *Int. J. Hydrogen Energy* **2008**, *33*, 2880–2890. [CrossRef]
74. Abanades, S.; Legal, A.; Cordier, A.; Peraudeau, G.; Flamant, G.; Julbe, A. Investigation of reactive cerium-based oxides for H2 production by thermochemical two-step water-splitting. *J. Mater. Sci.* **2010**, *45*, 4163–4173. [CrossRef]
75. Zhao, Z.; Uddi, M.; Tsvetkov, N.; Yildiz, B.; Ghoniem, A.F. Redox Kinetics Study of Fuel Reduced Ceria for Chemical-Looping Water Splitting. *J. Phys. Chem. C* **2016**, *120*, 16271–16289. [CrossRef]
76. Niazi, Z.; Irankhah, A.; Wang, Y.; Arandiyan, H. Cu, Mg and Co effect on nickel-ceria supported catalysts for ethanol steam reforming reaction. *Int. J. Hydrogen Energy* **2020**, *45*, 21512–21522. [CrossRef]
77. Zamar, F.; Trovarelli, A.; de Leitenburg, C.; Dolcetti, G. CeO 2-based solid solutions with the fluorite structure as novel and effective catalysts for methane combustion. *J. Chem. Soc. Chem. Commun.* **1995**, *9*, 965–966. [CrossRef]
78. Aggarwal, N.; Vasishth, A.; Singh, B.; Singh, B. Investigation of room temperature ferromagnetic behaviour in dilute magnetic oxides. *Integr. Ferroelectr.* **2018**, *186*, 10–16. [CrossRef]
79. Rougab, M.; Gueddouh, A. Light doping effects of rare-earth elements: Sc, Y, La and Lu in rockSalt AlN—first-principles study. *Appl. Phys. A* **2021**, *127*, 969. [CrossRef]
80. Orfila, M.; Linares, M.; Molina, R.; Botas, J.Á.; Sanz, R.; Marugán, J. Perovskite materials for hydrogen production by thermochemical water splitting. *Int. J. Hydrogen Energy* **2016**, *41*, 19329–19338. [CrossRef]

81. Scheffe, J.R.; Steinfeld, A. Oxygen exchange materials for solar thermochemical splitting of H_2O and CO_2: A review. *Mater. Today* **2014**, *17*, 341–348. [CrossRef]
82. Kaneko, H.; Ishihara, H.; Taku, S.; Naganuma, Y.; Hasegawa, N.; Tamaura, Y. Cerium ion redox system in $CeO_{2-x}Fe_2O_3$ solid solution at high temperatures (1273–1673 K) in the two-step water-splitting reaction for solar H_2 generation. *J. Mater. Sci.* **2008**, *43*, 3153–3161. [CrossRef]
83. Orfila, M.; Sanz, D.; Linares, M.; Molina, R.; Sanz, R.; Marugán, J.; Botas, J.Á. H_2 production by thermochemical water splitting with reticulated porous structures of ceria-based mixed oxide materials. *Int. J. Hydrogen Energy* **2021**, *46*, 17458–17471. [CrossRef]
84. Kaneko, H.; Miura, T.; Ishihara, H.; Taku, S.; Yokoyama, T.; Nakajima, H.; Tamaura, Y. Reactive ceramics of CeO2–MOx (M=Mn, Fe, Ni, Cu) for H2 generation by two-step water splitting using concentrated solar thermal energy. *Energy* **2007**, *32*, 656–663. [CrossRef]
85. Hao, Y.; Yang, C.-K.; Haile, S.M. Ceria–Zirconia Solid Solutions ($Ce_{1-x}Zr_xO_{2-\delta}$, $x \leq 0.2$) for Solar Thermochemical Water Splitting: A Thermodynamic Study. *Chem. Mater.* **2014**, *26*, 6073–6082. [CrossRef]
86. Chueh, W.C.; Haile, S.M. Ceria as a Thermochemical Reaction Medium for Selectively Generating Syngas or Methane from H_2O and CO_2. *ChemSusChem* **2009**, *2*, 735–739. [CrossRef]
87. Muhich, C.; Steinfeld, A. Principles of doping ceria for the solar thermochemical redox splitting of H_2O and CO_2. *J. Mater. Chem. A* **2017**, *5*, 15578–15590. [CrossRef]
88. Kuhn, M.; Bishop, S.R.; Rupp, J.L.M.; Tuller, H.L. Structural characterization and oxygen nonstoichiometry of ceria-zirconia ($Ce_{1-x}Zr_xO_{2-\delta}$) solid solutions. *Acta Mater.* **2013**, *61*, 4277–4288. [CrossRef]
89. Andersson, D.A.; Simak, S.I.; Skorodumova, N.V.; Abrikosov, I.A.; Johansson, B. Redox properties of CeO_2–MO_2 (M=Ti, Zr, Hf, or Th) solid solutions from first principles calculations. *Appl. Phys. Lett.* **2007**, *90*, 031909. [CrossRef]
90. Gokon, N.; Hasegawa, T.; Takahashi, S.; Kodama, T. Thermochemical two-step water-splitting for hydrogen production using Fe-YSZ particles and a ceramic foam device. *Energy* **2008**, *33*, 1407–1416. [CrossRef]
91. Weidenkaff, A.; Nüesch, P.; Wokaun, A.; Reller, A. Mechanistic studies of the water-splitting reaction for producing solar hydrogen. *Solid State Ion.* **1997**, *101–103*, 915–922. [CrossRef]
92. Cui, B.; Zhang, J.; Liu, S.; Liu, X.; Zhang, Z.; Sun, J. A low-temperature electro-thermochemical water-splitting cycle for hydrogen production based on $LiFeO_2$/Fe redox pair. *Int. J. Hydrogen Energy* **2020**, *45*, 20800–20807. [CrossRef]
93. Gokon, N.; Murayama, H.; Umeda, J.; Hatamachi, T.; Kodama, T. Monoclinic zirconia-supported Fe_3O_4 for the two-step water-splitting thermochemical cycle at high thermal reduction temperatures of 1400–1600 °C. *Int. J. Hydrogen Energy* **2009**, *34*, 1208–1217. [CrossRef]
94. Wegner, K.; Ly, H.C.; Weiss, R.J.; Pratsinis, S.E.; Steinfeld, A. In situ formation and hydrolysis of Zn nanoparticles for H2 production by the 2-step ZnO/Zn water-splitting thermochemical cycle. *Int. J. Hydrogen Energy* **2006**, *31*, 55–61. [CrossRef]
95. Gokon, N.; Mataga, T.; Kondo, N.; Kodama, T. Thermochemical two-step water splitting by internally circulating fluidized bed of NiFe2O4 particles: Successive reaction of thermal-reduction and water-decomposition steps. *Int. J. Hydrogen Energy* **2011**, *36*, 4757–4767. [CrossRef]
96. Gokon, N.; Mizuno, T.; Nakamuro, Y.; Kodama, T. Iron-Containing Yttria-Stabilized Zirconia System For Two-Step Thermochemical Water Splitting. *J. Sol. Energy Eng.* **2007**, *130*, 011018. [CrossRef]
97. Haeussler, A.; Abanades, S. Additive manufacturing and two-step redox cycling of ordered porous ceria structures for solar-driven thermochemical fuel production. *Chem. Eng. Sci.* **2021**, *246*, 116999. [CrossRef]
98. Petkovich, N.D.; Rudisill, S.G.; Venstrom, L.J.; Boman, D.B.; Davidson, J.H.; Stein, A. Control of Heterogeneity in Nanostructured Ce1–xZrxO2 Binary Oxides for Enhanced Thermal Stability and Water Splitting Activity. *J. Phys. Chem. C* **2011**, *115*, 21022–21033. [CrossRef]
99. Venstrom, L.J.; Petkovich, N.; Rudisill, S.; Stein, A.; Davidson, J.H. The Effects of Morphology on the Oxidation of Ceria by Water and Carbon Dioxide. *J. Sol. Energy Eng.* **2011**, *134*, 011005. [CrossRef]
100. Umeda, G.A.; Chueh, W.C.; Noailles, L.; Haile, S.M.; Dunn, B.S. Inverse opal ceria–zirconia: Architectural engineering for heterogeneous catalysis. *Energy Environ. Sci.* **2008**, *1*, 484–486. [CrossRef]
101. Stein, A.; Li, F.; Denny, N.R. Morphological Control in Colloidal Crystal Templating of Inverse Opals, Hierarchical Structures, and Shaped Particles. *Chem. Mater.* **2008**, *20*, 649–666. [CrossRef]
102. Reitzmann, A.; Bareiss, A.; Kraushaar-Czarnetzki, B. Simulation of a Reactor for the Partial Oxidation of o-Xylene to Phthalic Anhydride Packed with Ceramic Foam Monoliths. *Erdoel Erdgas Kohle* **2006**, *122*, 94–98.
103. Amar, V.; Puszynski, J.; Shende, R. H_2 generation from thermochemical water-splitting using yttria stabilized NiFe2O4 core-shell nanoparticles. *J. Renew. Sustain. Energy* **2015**, *7*, 023113. [CrossRef]
104. Amar, V.; Shende, R. Core-Shell Nanoscale Ferrite for Thermochemical Hydrogen Generation. In Proceedings of the TechConnect World Innovation Conference & Expo, Anaheim, CA, USA, 13–16 May 2018; 2018; pp. 148–151.
105. Amar, V.; Houck, J.; Maddipudi, B.; Shende, R. $NiFe_2O_4/ZrO_2$ Core-Shell Nanoparticles for Hydrogen Generation from Thermochemical Water-Splitting Process. *J. Catal. Chem. Eng. Adv.* **2020**, *7*, 105. [CrossRef]
106. Fresno, F.; Fernández-Saavedra, R.; Belén Gómez-Mancebo, M.; Vidal, A.; Sánchez, M.; Isabel Rucandio, M.; Quejido, A.J.; Romero, M. Solar hydrogen production by two-step thermochemical cycles: Evaluation of the activity of commercial ferrites. *Int. J. Hydrogen Energy* **2009**, *34*, 2918–2924. [CrossRef]